

pubs.acs.org/acsapm Article

# Ion-Selective Organic Electrochemical Transistor Sensors Using Molecularly Imprinted Polymers

Aaron B. Woeppel, Janessa Schaefer, Ho Joong Kim, Bryan W. Boudouris,\* and Stephen P. Beaudoin\*



Cite This: ACS Appl. Polym. Mater. 2022, 4, 6667-6674



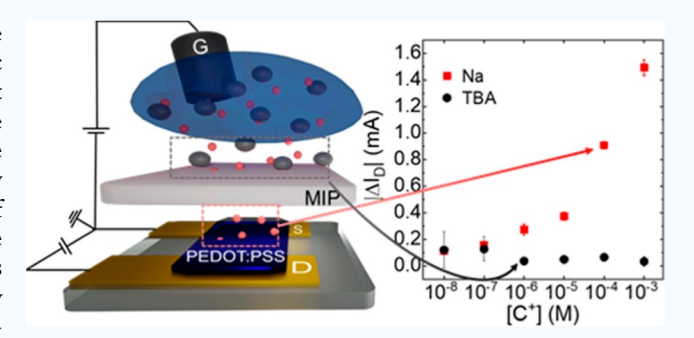
**ACCESS** 

Metrics & More

Article Recommendations

s Supporting Information

ABSTRACT: Organic electrochemical transistors (OECTs) have emerged as attractive candidates for biosensing and bioelectronic applications, and they show great potential to serve as compact platforms for ion analysis. OECTs contain electronically active polymer layers whose charge transport properties can be modulated by electrolytes possessing ion concentrations as low as 1  $\mu$ M. However, standard OECTs typically suffer from a lack of selectivity to electrolyte composition, a prerequisite for viable implementation into ion-sensing applications. To introduce this needed species selectivity, we have incorporated a molecularly imprinted polymer (MIP) into an OECT employing a poly(3,4-ethylene dioxythiophene) and poly(styrene sulfonate) polymer



blend (PEDOT:PSS) as the channel active layer material. The MIP-OECTs were challenged with three cations: the sodium ion, the ammonium ion, and the tetrabutylammonium ion. The MIP did not limit the performance of the OECT when gated with electrolytes containing sodium ions, but the barrier did reduce the gating capabilities of electrolytes containing ammonium ions and tetrabutylammonium ions due to size-exclusion effects. In particular, the MIP-OECT was not responsive to tetrabutylammonium ions at concentrations up to 1 mM. Additionally, electrolyte mixtures were used to test the potential for interference in MIP-OECTs. Ammonium ions produced negligible interference when detecting sodium ions; however, tetrabutylammonium ions completely suppressed the gating capabilities of sodium ions. This MIP-OECT platform demonstrates how electrolyte gating can be engineered to exhibit greater selectivity such that MIP-coated OECTs can be utilized as advanced sensor technologies.

KEYWORDS: organic electrochemical transistor, molecularly imprinted polymer, selective electrolyte gating, ion analysis, solution-phase sensor

# **■** INTRODUCTION

Distinguishing various dissolved salts in solution is critical in environmental science<sup>1-3</sup> (e.g., monitoring nitrate<sup>4-9</sup> and phosphate levels<sup>10,11</sup> in water), agriculture (e.g., determining nitrogen uptake by crops<sup>12,13</sup>), healthcare, and energetic material detection (e.g., identifying oxidizing agents in improvised explosives). Electrolyte-gated transistors are attractive candidates for these local sensing applications because of their mechanical robustness, compact form factors, and inexpensive module costs. In particular, organic electrochemical transistors (OECTs), a subset of electrolyte-gated transistors, have already shown promise, particularly in the field of biosensors, 14-19 and the physics behind their electrolyte gating allows for them to be readily adapted toward ion detection for other applications. A prototypical OECT structure contains a conductive polymer channel that can be reversibly oxidized or reduced via penetration of ions supplied by an electrolyte where the ion migration is controlled through the application of a gate voltage. This redox reaction changes the number of charge carriers, and the electrical conductivity of the polymer using a doping mechanism that is usually designed

to be reversible.  $^{20,21}$  Importantly, OECTs are extremely sensitive to the concentration of ions in solution with responsivities at concentrations as low as  $\sim 1~\mu M.^{22}$  However, the basic OECT performance is a function of the total ionic strength rather than of the electrolyte composition. While this drawback can be circumvented during the detection of neutral molecules, addressing the ion-selectivity of OECTs is a paramount concern for applications directed at ion analysis.

Previous efforts have shown success in using OECTs in this arena, and a handful of these OECTs have been supplemented with membranes to produce devices with enhanced ion-selective capability. <sup>23–28</sup> Importantly, the ion-selective membrane mechanism of action relies on the incorporation of complex organic molecules (i.e., ionophores) that are capable

Received: June 17, 2022 Revised: August 15, 2022 Accepted: August 16, 2022 Published: August 30, 2022





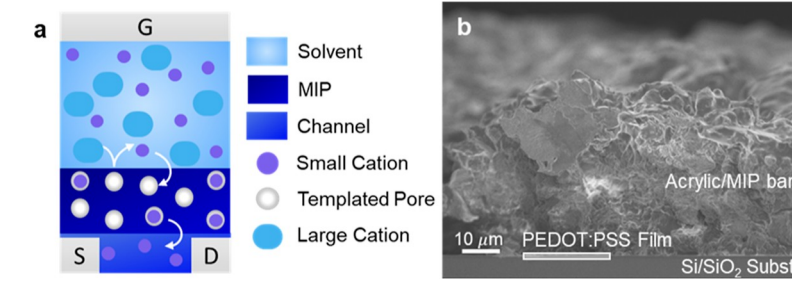


Figure 1. (a) Schematic structure of an OECT supplemented with a MIP barrier to introduce ion selectivity. (b) An SEM cross-sectional image of an acrylic bound MIP barrier atop a  $Si/SiO_2$  substrate coated with a  $\sim$ 80 nm thick PEDOT:PSS film.

of forming complexes with the desired target.<sup>29,30</sup> Such ionophore designs are established for common moieties (e.g., sodium ions,<sup>6</sup> potassium ions,<sup>8</sup> and copper ions<sup>12</sup>). However, the design of new ionophores draws heavily on time-intensive techniques of mimicking naturally occurring or previously discussed examples. 13 This results in large challenges in detecting new and unforeseen materials. More fundamentally, using principles that are similar to ion-selective electrodes, their ion selectivity results from changes to the membrane potential, which controls the effective gate bias, but the channel itself is not selectively gated by any particular ionic species. Therefore, these OECTs do not capture iondependent behavior that is produced by a non-selective counterpart. Although a mandatory component of the OECT, the electrolyte gate has received less interest despite its potential for solution analysis. The few examples include a membrane-free, ion-selective OECT that contained a gate electrode coated with a poly(3,4-ethylenedioxythiophene)based (PEDOT-based) polymer that contained thiophene monomers bearing either 18-crown-6 or 15-crown-5 pendant groups. Because of this chemical design strategy, the polymer coating was selectively permeable to either potassium ions or sodium ions resulting in selective gating.<sup>32</sup> Previously, a bilayer lipid membrane included an ion-transport protein to produce a charge selective barrier.<sup>33</sup> These efforts have pioneered the field of ion-selective gating, but there is potential to expand the application space and build new perspicacity behind new mechanisms of ion exclusion.

In fact, these successful efforts regarding ion-specific electrolyte gating have introduced the possibility associated with this technique for ion analysis, especially in the healthcare field. However, to expand into new application spaces, there is a need to assess the efficacy of applying new materials and methods to produce ion-exclusion. Molecularly imprinted polymers (MIPs) are a family of crosslinked polymers that are easy to synthesize and that can be designed to address these specific opportunities. MIPs are polymerized such that they contain template molecules that are later removed to form a nanoporous matrix. Their simple and inexpensive chemistry, along with potential for high selectivity, make them attractive for low-cost sensing applications. 34-37 In fact, MIPs have been incorporated into OECTs to serve as an active layer at either the channel or gate interface. 16,17,38 For instance, a MIP served as an ion barrier that became less permeable when it adsorbed target molecules, 16 and this produced a sensitive OECT sensor. However, there are no reports of MIPs being used to produce ion-selective OECTs where only specific ions effectively gate the device. Nevertheless, the design principles of the MIP can lend itself to make ion-exclusive OECTs. To this end, we demonstrate how a MIP can be incorporated into

an OECT to produce species-selective intercalation and gating. Rather than focusing on high electrolyte concentrations (i.e., from 1 mM to 1 M), 32,33,39 we turn our attention to lower concentration regimes as many of the aforementioned applications rely on detecting materials at sub-1 mM concentrations. For instance, the United States Environmental Protection Agency recommends levels of nitrate in water not exceed  $\sim 100 \ \mu M$  and levels of many metals (e.g., nickel and iron) remain less than 10 mg L<sup>-1.15</sup> Additionally, ammonium nitrate is a common oxidizer in improvised explosives. Commercial swabs are generally capable of only gathering several micrograms of explosive substance, this quantity of material would be insufficient to prepare 1-100 mM test solutions. 19,20 Our OECT performance is analyzed when gated with lower concentration electrolytes (i.e., ≤1 mM) and electrolyte mixtures. This demonstrates how the channel behaves when gated below the point of saturation and under the presence of interferents; as such, it points toward a new solution phase sensing archetype. 41,42

Specifically, we show a polymer-based OECT that incorporates a MIP to produce an ion-selective layer based on size exclusion. A PEDOT:PSS thin film serves as the channel material. Then, a poly(ethylene glycol dimethacrylate) (PEGDMA) MIP was cast directly atop the OECT. Importantly, this layer does not negatively impact the PEDOT:PSS performance nor does it significantly hinder the dynamics of the electrolyte gating. The selective properties of the OECT were benchmarked by evaluating the effectiveness of gating using electrolytes containing sodium ions or tetrabutylammonium ions at concentrations as low as 10 nM. Briefly, a sodium ion impacted the electrochemical performance of a MIP-coated PEDOT:PSS channel as effectively as it would gate an uncovered counterpart, even at concentrations <1 mM. However, the tetrabutylammonium ion was incapable of permeating the MIP and was ineffective at gating the coated channel at concentrations as high as 1 mM. Additionally, the potential for ion interference was established by introducing mixtures of either sodium ions and ammonium ions or sodium ions and tetrabutylammonium ions as potential electrolytic salts. Incorporating ammonium ions into a sodium-ion electrolyte gate had no significant impact on the channel performance. However, tetrabutylammonium ions were unable to permeate through the MIP, and instead they accumulated within the polymer barrier and prevented sodium ions from functioning as an electrolyte gate. In this way, we established the viability of incorporating a MIP into an OECT without diminishing sensitivity to concentrations <1 mM and introducing robust selectivity, even in the presence of interferents.

### RESULTS AND DISCUSSION

A MIP was incorporated as a barrier separating a PEDOT:PSS channel from its electrolyte gate (Figure 1a) to improve the ion selectivity of the OECT. This MIP was polymerized using a mixture containing a ratio of 1:4:45, isobutyl nitrite template molecules, allylurea monomers, and ethylene glycol dimethacrylate monomers. Following an overnight polymerization, the crosslinked polymer was ground into a fine powder and washed to remove the template molecules. The removal of template molecules yielded nanoscale pores capable of screening ions. The MIP was mixed with ethyl acetate and acrylic binder forming a slurry that was cast over the OECT channel producing a barrier <100  $\mu$ m in thickness (Figures 1b and S1). Isobutyl nitrite was selected as the template molecule because it is a neutral molecule with a molecular size that creates a proper pore architecture for controlling the ions that could permeate through the MIP and infiltrate the PEDOT:PSS channel. This template also contains an electron-withdrawing functional group capable of forming hydrogen-bonds with the allylurea functional monomer improving templating efficacy.9 In this way, only electrolytes with specific cations, such as sodium ions, effectively gated the MIP-OECTs. Moreover, water droplets formed contact angles of 25 and 100° atop a PEDOT:PSS film or a MIP coating, respectively, indicating that the MIP barrier was more hydrophobic than the PEDOT:PSS film (Figures S2 and S3). Previous work found that the MIP served as an ionic barrier when it was incorporated between OECT channel materials and electrolytes. <sup>16</sup> Before considering the selective properties introduced by the MIP barrier, the extent to which the MIP barrier altered OECT performance metrics, independent of the chosen electrolyte, was established.

First, to assess the potential contributions of introducing a MIP atop the OECT channel, the performances of both MIP-OECTs and their uncovered counterparts were evaluated. Here, sodium ions (Na<sup>+</sup>) were used to gate devices, and they were evaluated at room temperature using 100 mM NaNO3, a typical electrolyte concentration for OECTs.<sup>38–40</sup> In these measurements, the drain current  $(I_D)$  is tracked when the gate voltage  $(V_G)$  is swept at a constant drain voltage  $(V_D)$ . The uncovered OECT exhibited a peak transconductance (evaluated as  $\partial I_D/\partial V_G$ ) of 3.6 mS (Figure S4a) when the  $V_G$  was scanned at 6.67 mV s<sup>-1</sup>, a reasonable result for PEDOT:PSS OECTs.<sup>43</sup> The significance of the selected counterion was adjudicated by collecting additional transfer curves on a separate uncoated device gated with 100 mM NaCl, 100 mM NaNO<sub>3</sub>, and 50 mM Na<sub>2</sub>SO<sub>4</sub> (Figure S5a). The choice of anion had no notable impact on uncovered OECT performance. To further quantify the extent to which ionic charge is stored in the OECTs, the channel capacitance of 100 nF was determined using electrochemical impedance spectroscopy (Figure S6). This value is comparable to previously reported PEDOT:PSS OECTs. 43 The possibility of saturating these sensors during analysis of electrolytes possessing ionic concentrations of 1 mM was assessed by collecting cyclic voltammograms using a separate OECT and either 100 mM or 1 mM NaNO<sub>3</sub> aqueous solutions as the supporting electrolytes (Figure S7). Increasing the electrolyte concentration from 1 to 100 mM notably increased the currents collected throughout the voltammograms, indicating an increase in the magnitude of charge stored within the PEDOT:PSS channel. The increased charge storage is directly proportional to OECT transconductance and it implies that a 1 mM electrolyte was not saturating the OECT sensors. 20,44,45

The MIP-OECT performed similarly to the uncovered OECT as it produced nearly identical transfer, transconductance, and output curves (Figures 2, S4, and S8).

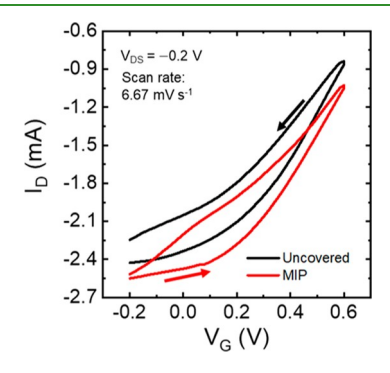


**Figure 2.** Representative transfer measurements for both uncovered (black,  $g_{m,max} = 3.6 \text{ mS}$ ) and composite (red,  $g_{m,max} = 4 \text{ mS}$ ) OECTs using 100 mM NaNO<sub>3</sub> as an electrolyte and a Ag/AgCl pellet as a gate electrode. The arrows indicate the direction in which gate voltage was scanned.

Incidentally, the MIP-OECT exhibited a transconductance of 4 mS, which is marginally greater than that produced by the uncovered OECT, but otherwise the two devices produce highly similar transconductance and this discrepancy is not attributed to contributions from the MIP. Instead, it highlights what one would anticipate as reasonable deviation from the average of multiple device measurements. To demonstrate this principle, transfer curves were collected on three adjacent channels coated by a common MIP film (Figure S9). These three channels showed similar variations, which were moderate, and they shared highly similar transconductance. The additional MIP OECT showed a weak differentiation between electrolytes of varying anions (Figure S5b). This variation however does not suggest that the MIP will inherently impact the OECT performance. These curves even suggest the potential selectivity of the MIP toward identifying anions. It is also notable that both covered and uncovered channels have a similar hysteretic behavior. Hysteresis is a common feature of electrolyte-gated transistors that respond to changes in gate-bias within seconds. 46 Hysteresis results from a discrepancy between the rate at which the  $V_G$  is scanned and that at which the ions in the electrolyte gate respond in the OECT. For sensing applications, the consideration of device hysteresis can be mitigated by applying a constant gate bias. 16,25 In this case, the dynamics governing transfer curve hysteresis would, instead, determine response time. The shared hysteretic behavior implies that the dynamics are driven by the transport limitations common in both devices. When gated with strong electrolytes, the electric field-driven transport through either the gate electrolyte or the PEDOT:PSS channel is responsible for limiting the device performance rather than transport through the MIP.

To begin assessing the MIP-OECT viability for ion detection, devices were gated with a more dilute (10  $\mu$ M) NaNO<sub>3</sub> aqueous electrolyte (Figure 3). The uncovered-OECT and MIP-OECT gated by a 10  $\mu$ M NaNO<sub>3</sub> electrolyte exhibited highly similar transconductance plots (Figure S4b) and they produced peak transconductances of 1.8 and 1.6 mS,

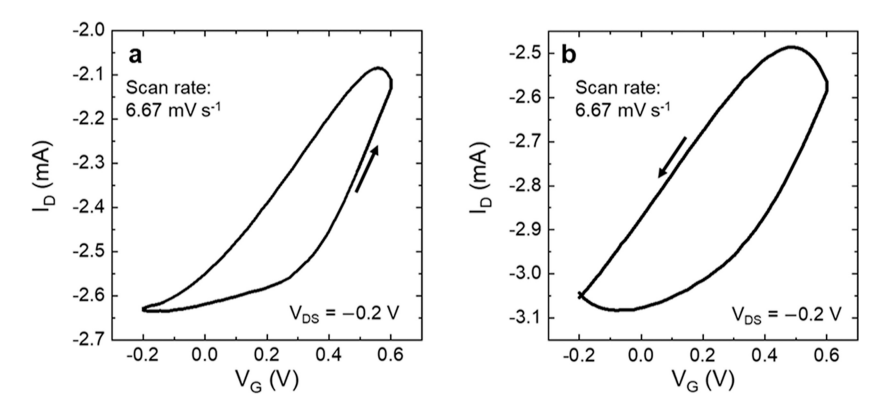


Figure 3. Representative transfer measurements for the (a) uncovered-OECT ( $g_{m,max} = 1.8 \text{ mS}$ ) and (b) MIP-OECT ( $g_{m,max} = 1.6 \text{ mS}$ ). A 10  $\mu$ M NaNO<sub>3</sub> aqueous solution was used to gate the OECTs. The arrows indicate that the direction gate voltage was swept.

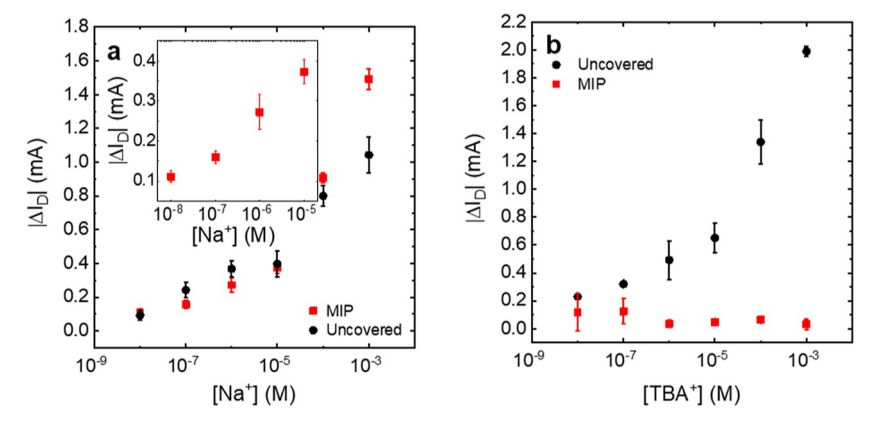


Figure 4. Comparison of calibration curves of an uncovered-OECT (black) and MIP-OECT (red) gated with (a) sodium ions and (b) tetrabutylammonium ions at a source-drain voltage of -0.2 V. The inset redisplays the MIP-OECT calibration curve between 10 nM and 10  $\mu$ M in concentration for a water-based solution. The OECT change in drain current is plotted as an absolute value.

respectively. Unsurprisingly, the transconductance values produced by these OECTs were lower in magnitude but of the same order of magnitude as those produced by OECTs gated with 100 mM solutions.

Additionally, the hysteresis between the forward and reverse scans increased rather significantly, indicating the OECT dynamics were slowed. One can expect the OECT will suffer from slower transport when analyzing more dilute electrolytes. The slowed dynamics are attributed to the slower ion transport associated with using a more dilute electrolyte. The impact of electrolyte strength on the device dynamics was seen over a range of concentrations (Figure S10a). Finally, the transfer curve produced by the MIP-OECT had a mildly greater hysteresis than the uncovered OECT when a 10  $\mu$ M aqueous electrolyte gate was employed. This effect was minor, and it is reasonable to expect that, even at micromolar-level concentrations, the MIP barrier will not control the dynamics exhibited by OECTs.

The MIP barrier does not negatively impact the OECT performance, but it does impart ion selectivity to the devices. To evaluate this idea, the MIP-OECT was challenged with the following salts: NaNO<sub>3</sub>, NH<sub>4</sub>NO<sub>3</sub>, and TBAClO<sub>4</sub>. These three electrolytes produced nearly identical performance gating a non-selective OECT (Figure S11). To compare the ion selectivity of the OECTs, particularly at lower ion concentrations, calibration curves were collected with both covered and uncovered OECTs (Figure 4). In collecting these curves, the OECT response was quantified as the total change in

magnitude of drain current ( $|\Delta I_D|$ ) exhibited after pulsing the OECT with a  $V_g=0.6$  V for 30 s. Note, a 30 s pulse produces a transient drain current rather than a steady (or pseudo-steady) result (Figure S10a). To weight the importance of obtaining a steady OECT response, a set of calibration curves was prepared after pulsing  $V_G$  for 120 s, a sufficiently long period to induce pseudo-steady currents (Figure S10). Naturally, the magnitude of transient  $\Delta I_D$  produced after 30 s differed from its steady-state counterpart. Nevertheless, both results demonstrated a potential limit of detection of ~100 nM for the three salts evaluated. The MIP-OECT has previously produced equal performance to the unselective OECTs (Figures 2 and 3). It is reasonable to expect the MIP-OECTs should be equally sensitive, and this 100 nM limit of detection will serve as a benchmark to judge the selective

When analyzing sodium ions, the MIP-OECT and uncovered-OECT produced calibration curves that showed similar features, particularly at low concentrations (Figure 4a). This reflects the results seen in the transfer characteristics shown in Figures 2 and 3. Also, as exhibited by the inset, the OECTs are sensitive and produce an electrolyte-gating response to concentrations and, indeed, maintained the same limit of detection ([Na<sup>+</sup>] = 100 nM) produced by the uncoated devices. The uncovered-OECT gated with tetrabutylammonium ions behaved similarly to the OECTs gated with sodium ions except with a larger magnitude of  $\Delta I_{\rm D}$  at higher concentrations. Notably, both the MIP-OECTs, when gated

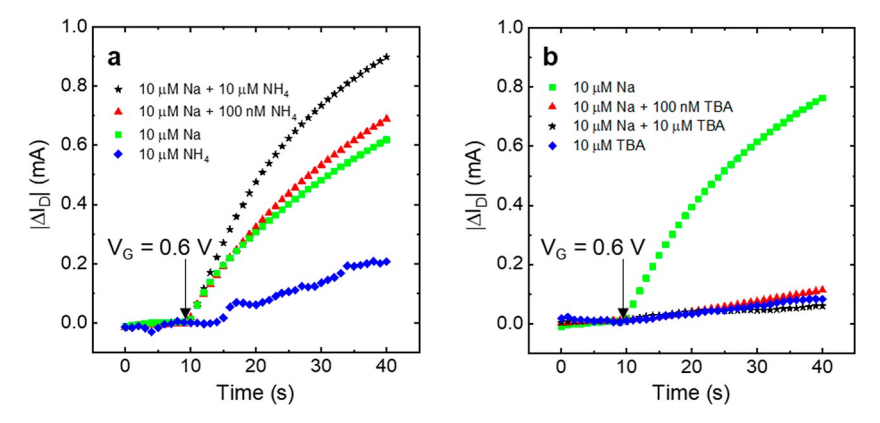


Figure 5. OECT responses produced by mixtures of either (a) sodium ions and ammonium ions or (b) sodium ions and tetrabutylammonium ions (TBA). OECT change in drain current is plotted as an absolute value. The arrow indicates that the gate bias of +0.6 V was introduced after 10 s.

with sodium nitrate electrolytes, and uncovered-OECTs, when gated with any of the three electrolytes considered, showed non-linear trends in their response to concentration changes (Figures 4 and S10). At low concentrations, increases in the  $\Delta I_{\rm D}$  are modest. As the concentration is increased to 10–100  $\mu\mathrm{M}$ , the increase in  $\Delta I_\mathrm{D}$  becomes more pronounced. This nonlinearity is attributed to the ratio between charge accumulation achievable by gating with a particular concentration to that which is required to saturate the channel. Meanwhile, the MIP-OECT was unresponsive to tetrabutylammonium ions, regardless of the concentration. Clearly the MIP is highly effective at screening these tetrabutylammonium ions at concentrations up to 1 mM (Figure 4b). The MIP-OECT, furthermore, exhibited reasonable selectivity when challenged with sodium ions and ammonium ions with 1 mM and 10 mM concentrations (Figure S12). While these MIP-OECTs were moderately less selective, they were still able to differentiate the solutions. We can expect that the MIP can effectively control which electrolyte moieties serve as the gating agents.

While these data establish the potential sensitivity and selectivity of the MIP-OECT, the potential for interference must be addressed. To judge this point, new OECTs were prepared and gated with mixtures of sodium ions and ammonium ions or mixtures of sodium ions and tetrabutylammonium ions (Figure 5). A singular OECT was used to judge either mixture, but to account for the dependence of the MIP-OECT on measurement history (Figure S13), measurements were acquired in order of increasing sodium ion concentration, and between each measurement, the MIP was removed and the wafer was cleaned by sequentially rinsing with acetone then isopropyl alcohol and then the wafer was immediately dried and a new MIP was cast. MIP-OECTs were first challenged with mixtures of sodium ions and ammonium ions (Figure 5a). The MIP-OECTs produced lower response when challenged with only ammonium ions than when challenged with sodium ions. While the ammonium ions ineffectively permeated through the MIP, it did not immediately prevent the sodium ions from passing. Contrary to the OECTs gated by mixtures of sodium ions and ammonium ions, those gated by mixtures of sodium ions and tetrabutylammonium ions were also non-responsive, as they were when gated by exclusively tetrabutylammonium ions (Figure 5b). The addition of tetrabutylammonium ions actively prevented sodium ions from permeating through the imprinted polymer. Ammonium ions did not prevent the sodium

transport, however. Tetrabutylammonium ions, but not ammonium ions, behaving as an interferent implies a physical difference in the extent to which either ion can permeate through the imprinted polymer.

The three electrolytes produced comparable dynamics when gating a non-selective OECT (Figure S11) implying no set ordering through which either ionic species moved through the electrolyte and penetrated an uncovered channel. Thus, the new dynamics resulting in potential interference is set by the transport through the MIP. The capability of the sodium ions to freely permeate through the MIP and its negligible impact on dynamics was previously established (Figures 2 through 4). The OECT dynamics are determined by either the ammonium ions or tetrabutylammonium ions. The modest response produced solely by ammonium ions implies that these ions have the potential to permeate through the MIP without significantly hindering permeability (i.e., without fouling) the MIP. The tetrabutylammonium ions are large enough that they cannot pass through the imprinted polymer, and they are believed to foul the imprinted polymer near the electrolyte-MIP interface. This interfacial phenomenon occurs on a length scale smaller than that of the thickness of the MIP. Thus, the fouling of the MIP should occur much more quickly than ion permeation through the entire MIP, and it would require a lower quantity of tetrabutylammonium ions than needed to effectively gate the channel. As such, once tetrabutylammonium ions are introduced (regardless of the concentration), they immediately prevent sodium ions from permeating into the channel, and the  $\Delta I_{\mathrm{D}}$  is suppressed. This fouling effect remained after rinsing the sensor and reintroducing an electrolyte free of tetrabutylammonium ions (Figure S13b), suggesting that the salt is captured in the MIP rather than accumulating in the electrolyte near the MIP surface. While the MIP had no impact on the performance of OECTs gated with electrolytes containing sufficiently small ionic species, it was either selectively impermeable or completely fouled by larger ions. The MIP-OECT was able to capture the sensitivity of an uncovered OECT which would be highly attractive for application toward solution analysis; it also introduced two unique sets of physics of interference when larger species were introduced.

# CONCLUSIONS

Ion-selective OECTs were prepared by adding an MIP barrier between a PEDOT:PSS channel and an aqueous electrolyte gate. The MIP OECTs showed equivalent transconductance to their uncovered counterparts when gated with either concentrated (100 mM) or dilute (10  $\mu$ M) aqueous electrolytes. At both concentrations, the MIP- and uncoated-OECTs displayed a similar hysteretic behavior. The MIP-OECTs show selectivity over a range of concentrations and can completely prevent the passage of tetrabutylammonium ions into the channel at concentrations  $\leq 1$  mM. Meanwhile, sub-1  $\mu$ M sodium ion electrolytes can weakly gate the device as they would an uncovered channel. The MIP slowed the drift of ammonium ions, but the cations were still capable of weakly gating the MIP OECT. Because of this, the ammonium ions do not impede the sodium ions permeation through the channel, and an electrolyte consisting of a mixture of the two ions was still effective at gating the OECT. Tetrabutylammonium ions, however, have no opportunity to permeate through the MIP. Instead, they begin to enter the MIP but immediately foul the MIP at the electrolyte interface. The length and time scale over which the MIP is fouled is shorter than that over which sodium ions can permeate through the entirety of the MIP and infiltrate the channel. Therefore, the sodium ions cannot access the polymer channel and a mixture of tetrabutylammonium ions and sodium ions is as ineffective an electrolyte gate as one of exclusively tetrabutylammonium ions. The MIP can introduce ion selectivity to an OECT by preventing ion moieties from acting as effective gating agents.

## METHODS

**Materials.** All chemicals were purchased from Sigma-Aldrich unless otherwise stated, and they were used as received. Isobutyl nitrite and allylurea were purchased from Tokyo Chemical Industry and used as received. Sodium nitrate was purchased from J. T. Baker and used as received. Glass substrates and silicon dioxide wafers were purchased from Mark Optics and Silicon Valley Microelectronics, respectively.

OECT Substrate Fabrication. OECTs were fabricated as reported previously with minor adjustments.<sup>44</sup> OECTs were prepared on either glass or on Si/SiO<sub>2</sub> substrates. Both materials were patterned following the same procedure and produced no notable difference in OECT performance. Wafers that were 4" in diameter were sonicated in toluene, acetone, and isopropanol in a sequential manner for 10 min each. Then, an AZ1518 photoresist was spun-coat atop the wafers. The photoresist mask was photolithographically patterned to yield the electrode geometry using a Karl Suss MA6 mask aligner beam, and the mask was developed in a mixture of water and MF CD-26 developer. Subsequently, a 5 nm thick layer of chromium and an 80 nm thick layer of gold were evaporated on the developed wafers in a sequential manner. Following metal deposition, the photoresist mask was removed by submerging the wafers overnight in N-methylpyrrolidone. Following the electrode patterning, a 1  $\mu$ m thick parylene-C insulating layer was deposited on the wafers using an SCS parylene CVD furnace and Silane A-174 served as an adhesion promotor between parylene-C and the wafer. Afterward, another round of photolithography was performed to pattern 500 × 20  $\mu$ m channels using AZ9260 photoresist, and the same alignment procedure described above with an AZ 400k developer. The parylene-C was etched using a March Jupiter II reactive ion etcher to expose the patterned channels. After spin-coating a final sacrificial layer of AZ1518, the wafer was diced with a DiscoDAD 641 dicing saw to produce the final substrates.

**MIP Synthesis.** The MIPs were fabricated by mixing ethylene glycol dimethacrylate (EGDMA), allylurea (AU), and isobutyl nitrite (IBN) template molecules. The polymerization was initiated with azobisisobutylnitrile (AIBN). In our experiments, a mixture of 5.66 mL of EGDMA (30 mmol), 267 mg of AU (2.67 mmol), 79  $\mu$ L of IBN (6.67 mmol), which resulted in a molar ratio of 1:4:45 IBN/AU/EGDMA, and 25 mg of AIBN were added to a reaction vessel under nitrogen. The vessel was stirred overnight at 60 °C to crosslink the

MIP. Then, the polymer was removed and mechanically ground with a mortar and pestle. The powder was then washed by stirring in a 100 mL mixture of acetic acid and methanol with a volume ratio of 8:2 for 24 h to remove the template molecules.

Device Preparation. Previously fabricated substrates were cleaned by sequentially rinsing with acetone and isopropanol and then plasma-cleaning for 5 min in a Harrick Plasma PDC-32G plasma cleaner. The PEDOT:PSS solution was prepared as previously reported in literature to improve conductivity and prevent delamination. 43,47 Briefly, the mixture contained 1 mL of 1.1% (by weight) conductive grade PEDOT:PSS, 50 µL of ethylene glycol, 25 mg of 3-(glycidoxypropyl) trimethoxysilane crosslinking agent, and 25 mg of dodecylbenzenesulfonic acid. The mixture was immediately spun-coat at 3000 rpm for 30 s on a cleaned substrate. An average film thickness of 80 nm was measured with a Bruker Instruments DektakXT profilometer. The polymer thin film was baked in air at 140 °C for 30 min on a hot plate. Uncovered (i.e., without the MIP layer) devices were rinsed with deionized water and tested. MIP coatings were prepared by combining 400 mg of acrylic binder, 200 mg of MIP (after grinding for a second time), and 1.2 mL of ethyl acetate. The vial was agitated, and 30  $\mu$ L was drop-cast on the device. Then, a doctor blade was used to spread the solution across the entire substrate aside from the contact pads. The device was then set on a hot plate at 60 °C for 1 min to dry in air.

**OECT Characterization.** OECT measurements were completed at room temperature and atmospheric pressure using a Lakeshore probe-station controlled by a Keysight Technologies B2902a source meter. A 1 mm diameter Ag/AgCl (Warner Instruments) pellet electrode was used as a gate electrode and submerged in 100  $\mu$ L of aqueous electrolyte contained in a PDMS well. To minimize potential contamination from the electrolyte, UHPLC-MS grade water (purchased from Sigma-Aldrich) was used to prepare electrolytes.

Calibration curves were acquired with each point constituting a mean and standard deviation for three consecutive measurements on the same channel. The channel was rinsed, and a new electrolyte gate was prepared between each measurement. The process of casting the MIP and binder adds unavoidable contamination. To accommodate this concern and mitigate the role of measurement order, the MIP-OECT was challenged with sodium solutions in an arbitrary order of concentrations and a sacrificial measurement was made before collecting data used for calibration which removed most contamination introduced by the MIP casting procedure or previous trials (Figure S14).

**Electrochemical Characterization.** Electrochemical measurements were collected using an electrode setup controlled by a Gamry Instruments Interface 1010E Potentiostat/Galvanostat. The source and drain electrodes were connected (i.e., shorted) to utilize the channel area as the working electrode and Ag/AgCl and a platinum coil were submerged in 10 mL of NaNO<sub>3</sub> (100 mM) to serve as reference and counter electrodes, respectively. Cyclic voltammograms were collected by sweeping from +0.5 to -0.5 V (and swept on the return from -0.5 to +0.5 V) at a rate of 10 mV s<sup>-1</sup>. Electrochemical impedance spectroscopy was completed using the same electrochemical setup with a DC bias of 0 V and an AC amplitude of 10 mV from 10<sup>5</sup> to 10<sup>1</sup> Hz. An equivalent capacitance was gathered from electrochemical impedance spectroscopy using Gamry Echem Analyst Software to fit an equivalent circuit consisting of a constant phase element and bound Warburg impedance element.

SEM Specimen Preparation and Imaging. Scanning electron microscopy (SEM) samples were prepared on silicon substrates mechanically cleaved into 1 cm² slides. After dicing, the slides were cleaned by sonicating for 10 min each, in acetone, chloroform, and isopropanol, in a sequential manner, followed by plasma cleaning for 5 min. A layer of PEDOT:PSS and MIP coating were deposited as described above. The wafer was, again, cleaved to produce a cross section. Subsequently, a layer of carbon coating was sputter coated atop the MIP using an SPI sputter coater. SEM images were collected using a Hitachi S 4800 field emission scanning electron microscope. The secondary emission image was collected using a 1.3 kV and 4.7  $\mu$ A electron beam.

**Contact Angle Measurements.** Selective and non-selective OECTs used for contact angle measurements were prepared as reported above on Si/SiO $_2$  substrates coated with parylene-C. Contact angle measurements were then acquired at 20 °C using 10  $\mu$ L drops of water and measured using a Krüss DSA 100S Drop Shape Analyzer.

### ASSOCIATED CONTENT

# Supporting Information

The Supporting Information is available free of charge at https://pubs.acs.org/doi/10.1021/acsapm.2c01030.

Additional SEM images of the MIP cross-section; water contact angle measurements atop MIP and PEDOT:PSS films; cyclic voltammetry and electrochemical impedance spectroscopy data; uncovered and MIP-OECT output measurements; unselective OECT time-dependent measurements and calibration curve; re-tested MIP-OECT time-dependent measurements; and time-dependent MIP-OECT data used to construct the calibration curve (PDF)

# AUTHOR INFORMATION

#### **Corresponding Authors**

Bryan W. Boudouris — Charles D. Davidson School of Chemical Engineering, Purdue University, West Lafayette, Indiana 47907, United States; Purdue Energetics Research Center and Department of Chemistry, Purdue University, West Lafayette, Indiana 47907, United States; orcid.org/0000-0003-0428-631X; Email: boudouris@purdue.edu

Stephen P. Beaudoin — Charles D. Davidson School of Chemical Engineering, Purdue University, West Lafayette, Indiana 47907, United States; Purdue Energetics Research Center, Purdue University, West Lafayette, Indiana 47907, United States; Email: sbeaudoi@purdue.edu

# **Authors**

Aaron B. Woeppel — Charles D. Davidson School of Chemical Engineering, Purdue University, West Lafayette, Indiana 47907, United States; Purdue Energetics Research Center, Purdue University, West Lafayette, Indiana 47907, United States; orcid.org/0000-0003-3067-528X

Janessa Schaefer – Charles D. Davidson School of Chemical Engineering, Purdue University, West Lafayette, Indiana 47907, United States

**Ho Joong Kim** – Charles D. Davidson School of Chemical Engineering, Purdue University, West Lafayette, Indiana 47907, United States

Complete contact information is available at: https://pubs.acs.org/10.1021/acsapm.2c01030

# **Author Contributions**

A.B.W. designed experiments, synthesized the MIPs, prepared and tested OECTs, and prepared this manuscript. J.S. assisted in collecting OECT measurements. H.J.K designed and fabricated device substrates. B.W.B. and S.P.B. conceived the project and directed research and manuscript preparation. All authors have given approval to the final version of the manuscript.

# **Notes**

The authors declare no competing financial interest.

### ACKNOWLEDGMENTS

This work was primarily supported through the National Science Foundation (NSF) National Robotics Initiative (NRI) under Award 1925194. A.B.W. acknowledges the National Science Foundation for support under the Graduate Research Fellowship Program (GRFP) under Award DGE-1842166.

# REFERENCES

- (1) Dwivedi, U. N.; Mishra, S.; Singh, P.; Tripathi, R. D. Nitrate Pollution and Its Remediation. *Environmental Bioremediation Technologies*; Springer, 2007.
- (2) Clapp, C. E.; Liu, R.; Linden, D. R.; Larson, W. E.; Dowdy, R. H. Nitrates in Soils and Waters from Sewage Wastes on Land. *Managing Risks of Nitrates to Humans and the Environment*; Woodhead Publishing, 1999.
- (3) Ambulkar, A. R. Nutrient Pollution and Wastewater Treatment Systems. Oxford Research Encyclopedia of Environmental Science; Oxford University Press, 2017.
- (4) Essousi, H.; Barhoumi, H.; Bibani, M.; Ktari, N.; Wendler, F.; Al-Hamry, A.; Kanoun, O. Ion-Imprinted Electrochemical Sensor Based on Copper Nanoparticles-Polyaniline Matrix for Nitrate Detection. *J. Sens.* **2019**, 2019, 4257125.
- (5) Muntean, E.; Mihaiescu, T. Groundwater Quality Studies in Two Transylvanian Rural Communities Using Parallel Ion Chromatography. *Environ. Eng. Manag. J.* **2016**, *15*, 2703.
- (6) Liu, S.; Che, H.; Smith, K.; Chen, C. A Method of Detecting Contamination Events Using Multiple Conventional Water Quality Sensors. *Environ. Monit. Assess.* **2015**, *187*, 4189.
- (7) Chen, X.; Pu, H.; Fu, Z.; Sui, X.; Chang, J.; Chen, J.; Mao, S. Real-Time and Selective Detection of Nitrates in Water Using Graphene-Based Field-Effect Transistor Sensors. *Environ. Sci.: Nano* **2018**, *5*, 1990.
- (8) Zhou, Y.; Ma, M.; He, H.; Cai, Z.; Gao, N.; He, C.; Chang, G.; Wang, X.; He, Y. Highly Sensitive Nitrite Sensor Based on AuNPs/RGO Nanocomposites Modified Graphene Electrochemical Transistors. *Biosens. Bioelectron.* **2019**, *146*, 111751.
- (9) Alahi, M. E. E.; Mukhopadhyay, S. C.; Burkitt, L. Imprinted Polymer Coated Impedimetric Nitrate Sensor for Real-Time Water Quality Monitoring. *Sens. Actuators, B* **2018**, 259, 753.
- (10) Kugimiya, A.; Takei, H. Selective Recovery of Phosphate from River Water Using Molecularly Imprinted Polymers. *Anal. Lett.* **2008**, 41, 302.
- (11) Kugimiya, A.; Takei, H. Preparation of Molecularly Imprinted Polymers with Thiourea Group for Phosphate. *Anal. Chim. Acta* **2006**, 564, 179.
- (12) Finch, H. J. S.; Samuel, A. M.; Lane, G. P. F. Fertilisers and Manures. Lockhart & Wiseman's Crop Husbandry Including Grassland; Woodhead Publishing, 2014.
- (13) Sangare, S. K.; Compaore, E.; Buerkert, A.; Vanclooster, M.; Sedogo, M. P.; Bielders, C. L. Field-Scale Analysis of Water and Nutrient Use Efficiency for Vegetable Production in a West African Urban Agricultural System. *Nutr. Cycling Agroecosyst.* **2012**, 92, 207.
- (14) Lin, P.; Luo, X.; Hsing, I. M.; Yan, F. Organic Electrochemical Transistors Integrated in Flexible Microfluidic Systems and Used for Label-Free DNA Sensing. *Adv. Mater.* **2011**, 23, 4035.
- (15) Ji, X.; Lau, H. Y.; Ren, X.; Peng, B.; Zhai, P.; Feng, S. P.; Chan, P. K. L. Highly Sensitive Metabolite Biosensor Based on Organic Electrochemical Transistor Integrated with Microfluidic Channel and Poly(N-Vinyl-2-Pyrrolidone)-Capped Platinum Nanoparticles. *Adv. Mater. Technol.* **2016**, *1*, 1600042.
- (16) Parlak, O.; Keene, S. T.; Marais, A.; Curto, V. F.; Salleo, A. Molecularly Selective Nanoporous Membrane-Based Wearable Organic Electrochemical Device for Noninvasive Cortisol Sensing. *Sci. Adv.* **2018**, *4*, No. eaar2904.
- (17) Zhang, L.; Wang, G.; Wu, D.; Xiong, C.; Zheng, L.; Ding, Y.; Lu, H.; Zhang, G.; Qiu, L. Highly Selective and Sensitive Sensor Based on an Organic Electrochemical Transistor for the Detection of Ascorbic Acid. *Biosens. Bioelectron.* **2018**, *100*, 235.

- (18) Koklu, A.; Wustoni, S.; Musteata, V.-E.; Ohayon, D.; Moser, M.; McCulloch, I.; Nunes, S. P.; Inal, S. Microfluidic Integrated Organic Electrochemical Transistor with a Nanoporous Membrane for Amyloid-β Detection. ACS Nano 2021, 15, 8130.
- (19) Tang, H.; Yan, F.; Lin, P.; Xu, J.; Chan, H. L. W. Highly Sensitive Glucose Biosensors Based on Organic Electrochemical Transistors Using Platinum Gate Electrodes Modified with Enzyme and Nanomaterials. *Adv. Funct. Mater.* **2011**, *21*, 2264.
- (20) Bernards, D. A.; Malliaras, G. G. Steady-State and Transient Behavior of Organic Electrochemical Transistors. *Adv. Funct. Mater.* **2007**, *17*, 3538.
- (21) Kaphle, V.; Paudel, P. R.; Dahal, D.; Radha Krishnan, R. K.; Lüssem, B. Finding the Equilibrium of Organic Electrochemical Transistors. *Nat. Commun.* **2020**, *11*, 2515.
- (22) Wang, N.; Liu, Y.; Fu, Y.; Yan, F. AC Measurements Using Organic Electrochemical Transistors for Accurate Sensing. ACS Appl. Mater. Interfaces 2018, 10, 25834.
- (23) Keene, S. T.; Fogarty, D.; Cooke, R.; Casadevall, C. D.; Salleo, A.; Parlak, O. Wearable Organic Electrochemical Transistor Patch for Multiplexed Sensing of Calcium and Ammonium Ions from Human Perspiration. *Adv. Healthcare Mater.* **2019**, *8*, 1901321.
- (24) Sessolo, M.; Rivnay, J.; Bandiello, E.; Malliaras, G. G.; Bolink, H. J. Ion-Selective Organic Electrochemical Transistors. *Adv. Mater.* **2014**, *26*, 4803.
- (25) Han, S.; Yamamoto, S.; Polyravas, A. G.; Malliaras, G. G. Microfabricated Ion-Selective Transistors with Fast and Super-Nernstian Response. *Adv. Mater.* **2020**, *32*, 2004790.
- (26) Pierre, A.; Doris, S. E.; Lujan, R.; Street, R. A. Monolithic Integration of Ion-Selective Organic Electrochemical Transistors with Thin Film Transistors on Flexible Substrates. *Adv. Mater. Technol.* **2019**, *4*, 1800577.
- (27) Koutsouras, D. A.; Lieberth, K.; Torricelli, F.; Gkoupidenis, P.; Blom, P. W. M. Selective Ion Detection with Integrated Organic Electrochemical Transistors. *Adv. Mater. Technol.* **2021**, *6*, 2100591.
- (28) Mousavi, Z.; Ekholm, A.; Bobacka, J.; Ivaska, A. Ion-Selective Organic Electrochemical Junction Transistors Based on Poly(3,4-Ethylenedioxythiophene) Doped with Poly(Styrene Sulfonate). *Electroanalysis* **2009**, 21, 472.
- (29) Oliveri, V. Biomedical Applications of Copper Ionophores. Coord. Chem. Rev. 2020, 422, 213474.
- (30) Johnson, R. D.; Bachas, L. G. Ionophore-Based Ion-Selective Potentiometric and Optical Sensors. *Anal. Bioanal. Chem.* **2003**, *376*, 328–341.
- (31) Bobacka, J. Conducting Polymer-Based Solid-State Ion-Selective Electrodes. *Electroanalysis* **2006**, *18*, 7.
- (32) Wustoni, S.; Combe, C.; Ohayon, D.; Akhtar, M. H.; McCulloch, I.; Inal, S. Membrane-Free Detection of Metal Cations with an Organic Electrochemical Transistor. *Adv. Funct. Mater.* **2019**, 29, 1904403.
- (33) Bernards, D. A.; Malliaras, G. G.; Toombes, G. E. S.; Gruner, S. M. Gating of an Organic Transistor through a Bilayer Lipid Membrane with Ion Channels. *Appl. Phys. Lett.* **2006**, *89*, 053505.
- (34) Bunte, G.; Hürttlen, J.; Pontius, H.; Hartlieb, K.; Krause, H. Gas Phase Detection of Explosives Such as 2,4,6-Trinitrotoluene by Molecularly Imprinted Polymers. *Anal. Chim. Acta* **2007**, *591*, 49.
- (35) Ahmad, O. S.; Bedwell, T. S.; Esen, C.; Garcia-Cruz, A.; Piletsky, S. A. Molecularly Imprinted Polymers in Electrochemical and Optical Sensors. *Trends Biotechnol.* **2019**, *37*, 294.
- (36) George, S. J.; Ajayaghosh, A. Self-Assembled Nanotapes of Oligo(p-phenylene vinylene)s: Sol-Gel-Controlled Optical Properties in Fluorescent  $\pi$ -Electronic Gels. *Chem.—Eur. J.* **2005**, *11*, 3217.
- (37) Lu, W.; Xue, M.; Xu, Z.; Dong, X.; Xue, F.; Wang, F.; Wang, Q.; Meng, Z. Molecularly Imprinted Polymers for the Sensing of Explosives and Chemical Warfare Agents. *Curr. Org. Chem.* **2015**, *19*, 62.
- (38) Zhang, L.; Wang, G.; Xiong, C.; Zheng, L.; He, J.; Ding, Y.; Lu, H.; Zhang, G.; Cho, K.; Qiu, L. Chirality Detection of Amino Acid Enantiomers by Organic Electrochemical Transistor. *Biosens. Bioelectron.* **2018**, *105*, 121.

- (39) Tseng, H.; Cucchi, M.; Weissbach, A.; Leo, K.; Kleemann, H. Membrane-Free, Selective Ion Sensing by Combining Organic Electrochemical Transistors and Impedance Analysis of Ionic Diffusion. ACS Appl. Electron. Mater. 2021, 3, 3898.
- (40) Environmental Protection Agency. 816-F-09-004. National Primary Drinking Water Regulation. last revised May 2009, https://www.epa.gov/sdwa/drinking-water-regulations-and-contaminants#Primary (accessed Aug 07, 2022).
- (41) Fisher, D.; Zach, R.; Matana, Y.; Elia, P.; Shustack, S.; Sharon, Y.; Zeiri, Y. Bomb Swab: Can Trace Explosive Particle Sampling and Detection Be Improved? *Talanta* **2017**, *174*, 92.
- (42) Laster, J. Ś.; Ezeamaku, C. D.; Beaudoin, S. P.; Boudouris, B. W. Impact of Surface Chemistry on the Adhesion of an Energetic Small Molecule to a Conducting Polymer Surface. *Colloids Surf., A* **2018**, *551*, 74.
- (43) Rivnay, J.; Leleux, P.; Ferro, M.; Sessolo, M.; Williamson, A.; Koutsouras, D. A.; Khodagholy, D.; Ramuz, M.; Strakosas, X.; Owens, R. M.; Benar, C.; Badier, J. M.; Bernard, C.; Malliaras, G. G. High-Performance Transistors for Bioelectronics through Tuning of Channel Thickness. *Sci. Adv.* 2015, *1*, No. e1400251.
- (44) Kim, H. J.; Perera, K.; Liang, Z.; Bowen, B.; Mei, J.; Boudouris, B. W. Radical Polymer-Based Organic Electrochemical Transistors. *ACS Macro Lett.* **2022**, *11*, 243.
- (45) Bianchi, M.; Carli, S.; Di Lauro, M.; Prato, M.; Murgia, M.; Fadiga, L.; Biscarini, F. Scaling of capacitance of PEDOT:PSS: volume vs. area. *J. Mater. Chem. C* **2020**, *8*, 11252.
- (46) Faria, G. C.; Duong, D. T.; Salleo, A. On the Transient Response of Organic Electrochemical Transistors. *Org. Electron.* **2017**, 45, 215.
- (47) Khodagholy, D.; Curto, V. F.; Fraser, K. J.; Gurfinkel, M.; Byrne, R.; Diamond, D.; Malliaras, G. G.; Benito-Lopez, F.; Owens, R. M. Organic Electrochemical Transistor Incorporating an Ionogel as a Solid State Electrolyte for Lactate Sensing. *J. Mater. Chem.* **2012**, 22, 4440

# ☐ Recommended by ACS

# n-Type Organic Electrochemical Transistors with High Transconductance and Stability

Yazhou Wang, Wan Yue, et al. JANUARY 08, 2023

CHEMISTRY OF MATERIALS

READ 🗹

# Gradual Morphological Change in PEDOT:PSS Thin Films Immersed in an Aqueous Solution

Inwoo Lee, Changhun Yun, et al.

JANUARY 13, 2023

LANGMUIR

READ 🗹

# Adhesive Properties of Semiconducting Polymers: Poly(3-alkylthiophene) as an Ersatz Glue

Alexander X. Chen, Darren J. Lipomi, et al.

APRIL 04, 2023

CHEMISTRY OF MATERIALS

READ 🗹

# Interactions of Catalytic Enzymes with n-Type Polymers for High-Performance Metabolite Sensors

David Ohayon, Sahika Inal, et al.

FEBRUARY 07, 2023

ACS APPLIED MATERIALS & INTERFACES

READ 🗹

Get More Suggestions >